How Some Simple Solids Hold Together. The Use of the Fragment Formalism in Crystal Chemistry

Jeremy K. Burdett[1]

Contribution from the Department of Chemistry, The University of Chicago, Chicago, Illinois 60637. *Received June 11, 1979*

Abstract: The fragment formalism, widely used in viewing the structures of inorganic and organometallic molecules, is used to view the structures of some simple solids based on the packing of planar hexagonal 6^3 sheets (viz., graphite) and their puckered analogues. Using the frontier orbitals of an $A_3X_3H_6$ unit, puckered sheets in solid-state AX structures are predicted to link via XX, AX, and AA contacts in systems containing seven, eight, and nine electrons per AX formula unit. These features are indeed found experimentally for the Cu^1S part of covellite, a whole range of eight electron wurtzites and sphalerites (e.g., ZnS, AlN, $LiGaO_2$) and GaX (X = chalcogen) species, respectively. The correct site preferences in the GaX species and thus the presence of Ga–Ga linkages is also implied by the charge distribution calculated for a fragment of the structure. The bond overlap populations calculated for puckered six-membered $A_3X_3H_6$ rings in chair and boat conformations are in the same order as the bond lengths in wurtzites and sphalerites where these fragments are found linked together. The calculations predict r_v(wurtzite) > r(sphalerite) > r_0(wurtzite) and this is matched by the experimental bond lengths. The puckered sheet becomes less energetically unfavorable compared to the planar analogue as the electronegativity difference ($\Delta\chi$) between A and X increases. In addition the boat conformation becomes less unstable compared to the chair conformation. Both results are in accord with the greater prevalence in practice of the wurtzite structure (containing chairs and boats) compared to the sphalerite structure as $\Delta\chi$ increases. The experimental trends in the ratio r_v/r_o in the wurtzites with increasing $\Delta\chi$ are also matched by these changes in bond overlap populations. Use of the fragment formalism also shows why the cadmium halide structures hold together with the most electronegative species (halide) sandwiching the metal in the 16-electron case (e.g., $CdCl_2$) but in the opposite fashion in the inverse structure (e.g., Cs_2O) for eight-electron systems. The MoS_2, AlB_2, $CaSi_2$, delafossite, and NiAs structures may be assembled in similar ways.

Introduction

In contrast to theoretical studies of molecules in recent years, which have ranged from the full numerology of ab initio methods to simple symmetry and perturbation arguments, theoretical studies of the structures of infinite solids have emphasized rather different aspects.[2,3] Band structure calculations have helped quantitatively correlate bulk electrical and magnetic properties with structure and composition, high-quality calculations[4] on fragments removed from the lattice have enabled quantitative comparisons with photoelectron studies of the solid, and the results of simpler calculations on fragments have been found[5] to mimic bond length–bond angle correlations in tetrahedrally coordinated (especially silicate) systems. Very little attention has been paid, however, to the development of simple molecular orbital arguments of the type which today form the cornerstone of much of molecular organic and inorganic chemistry. We have recently shown[6] how the Wade scheme[7] for polyhedral *molecular* systems, with its closo, nido, and arachno cages, has strong resemblances to traditional ways crystal chemists have viewed[8] defect and stuffed derivatives of simple crystal types. We also showed how the principles involved in relating the structures of electron-rich systems to those of their electron-precise analogues are equally applicable to molecules[9] and solids. In this paper we show how the fragment formalism,[10] now widely used to view the structures of inorganic and organometallic molecules, may profitably be used to examine the electronic structure of extended arrays. We shall limit ourselves in this paper to structures derived from planar 6^3 sheets,[11] such as those found in the graphite and isoelectronic borazine structures, and its puckered analogue.

Molecular Orbital Structure of the 6^3 Sheet

Compared to molecules the theoretical study of solid-state structures is much more difficult from both the computational and conceptual viewpoint, because of the size of the structure to be considered. However, crystal chemists have used a localized orbital basis to view the structures of solids since Pauling's early and vital contributions to the solid state.[13] Thus the cubic diamond structure contains carbon atoms which make use of four hybrid orbitals pointing to the vertices of a tetrahedron, just as a carbon atom in a large steroid molecule or in methane itself. We shall not use this traditional localized viewpoint here but will examine instead the molecular orbitals of a fragment of the crystal structure, chosen to represent both the local symmetry and stoichiometry of the extended array. Rather than focus on the exact quantum molecular numerology of the fragment (as Tossell and co-workers have done,[4] for example, in correlating the observed photoelectron spectrum of solid FeO with calculations on the fragment FeO_6^{-10}) we shall examine the orbital properties of the fragment from a symmetry and energy point of view with the aim of understanding how the fragment interacts with other species to generate an infinite array.

For the 6^3 sheet (**1**) the smallest structural fragment is a regular hexagon of atoms, terminated with hydrogen atoms

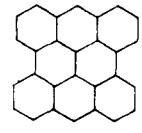

1

to simulate its attachment to the rest of the sheet—i.e., the benzene molecule. The molecular orbitals of this species are well known[14] and may be divided into those associated with the in-plane σ-type interactions and those associated with out-of-plane π-type interactions (Figure 1). On puckering the ring such that the bond angles become tetrahedral, this separability is lost. Figure 1 shows how the π and π^* orbital energies for an A_6H_6 unit change as it is distorted to chair and boat arrangements. (The symmetry and overlap arguments we shall mainly use in this paper are supported by numerical calculations of the extended Hückel type. The parameters used in the calculations are given in the Appendix). The σ,π separability is lost and on a localized orbital basis directional orbitals are formed which point to the vacant coordination site of each carbon atom (**2**). Of use to us later will be the form of the orbitals in a $A_3X_3H_6$ ring made up of alternately A and X atoms where X is more electronegative (i.e., its atomic orbitals

0002-7863/80/1502-0450$01.00/0

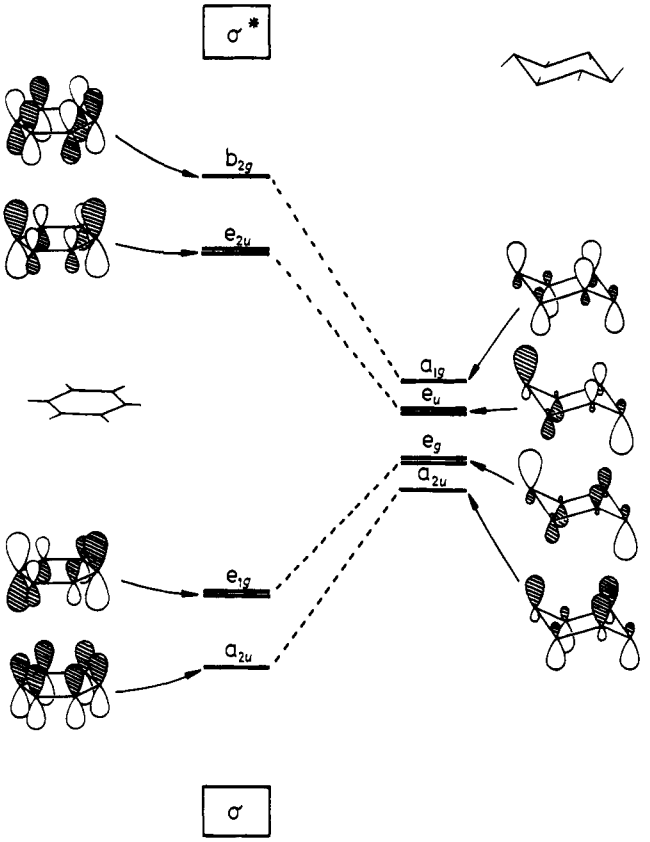

Figure 1. Valence orbitals of benzene ring—and how they change in energy as the ring is puckered. Only the orbitals derived from the π and π^* benzene orbitals are shown. There are 12 σ and 12 σ^* orbitals represented in this diagram as blocks (six involved in CC and six in CH linkages). With a total of eight electrons per formula unit all the orbitals through e_{1g} of the planar molecule or e_g of the puckered molecule are doubly filled with electrons.

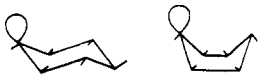

2

lie at higher ionization potential) than A. Figure 2 shows how the relative energy of the orbitals and their descriptions change relative to the A_6H_6 unit. The A–X bonding orbitals contain more X than A character and the converse is true for the antibonding orbitals. Clearly all the low-energy orbitals in the planar and puckered sheets are filled if eight electrons are contributed by each AX formula unit. For this case it is energetically unprofitable for an *isolated* planar sheet to distort since the occupied π bonding orbitals are destabilized. (As we shall see later, however, puckered sheets with this electron configuration can link together to form infinite three-dimensional structures.) With ten electrons per AX unit, however, the extra six electrons occupy the π^* orbitals of the planar unit which are rapidly stabilized on bending. Since antibonding interactions are generally larger than their bonding counterparts the stabilization afforded the π^* orbitals in this process will be larger than the destabilization experienced by the π orbitals. Elemental arsenic[15] with this electronic configuration does indeed consist of puckered sheets of atoms. Antimony and bismuth have similar structures. Black phosphorus has a closely related structure where the puckered six-membered rings are linked together in a slightly different way.

Linking of Puckered Sheets

The frontier orbitals of the puckered sheet are clearly those orbitals derived (Figures 1 and 2) from the π-type orbitals of

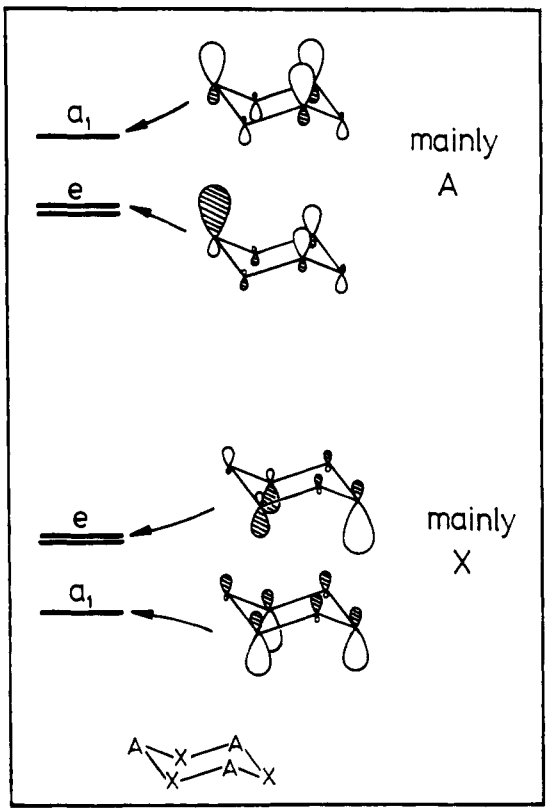

Figure 2. The orbitals of a puckered $A_3X_3H_6$ unit (electronegativity of X greater than that of A).

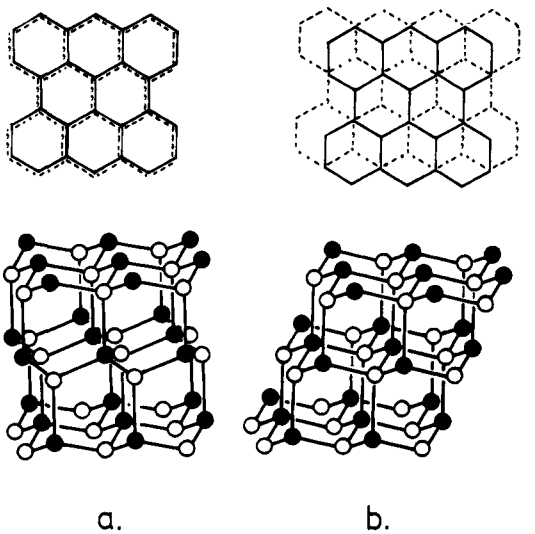

Figure 3. Packing of puckered sheets: (a) eclipsed arrangement giving rise to the wurtzite structure; (b) staggered arrangement giving rise to the sphalerite (or zincblende) structure.

the planar geometry. There are two basic ways sheets based on **1** may be stacked one on top of the next. A layer either eclipses (E) or is staggered (S) relative to the one beneath it (Figure 3). The sequence EEE . . . gives rise to the wurtzite structure of ZnS (and its parent structure, hexagonal diamond or lonsdaleite, where all the atoms are equivalent) and the sequence SSS . . . gives rise to the sphalerite (or zincblende) structure of ZnS (and its parent structure, cubic diamond). There are many other polymorphs of ZnS obtained by stacking the sheets in different ways. In the SiC system some of these give rise to the carborundum structures. We shall concentrate on the sphalerite and wurtzite structures here. Of particular importance is that, in stacking these horizontal puckered sheets

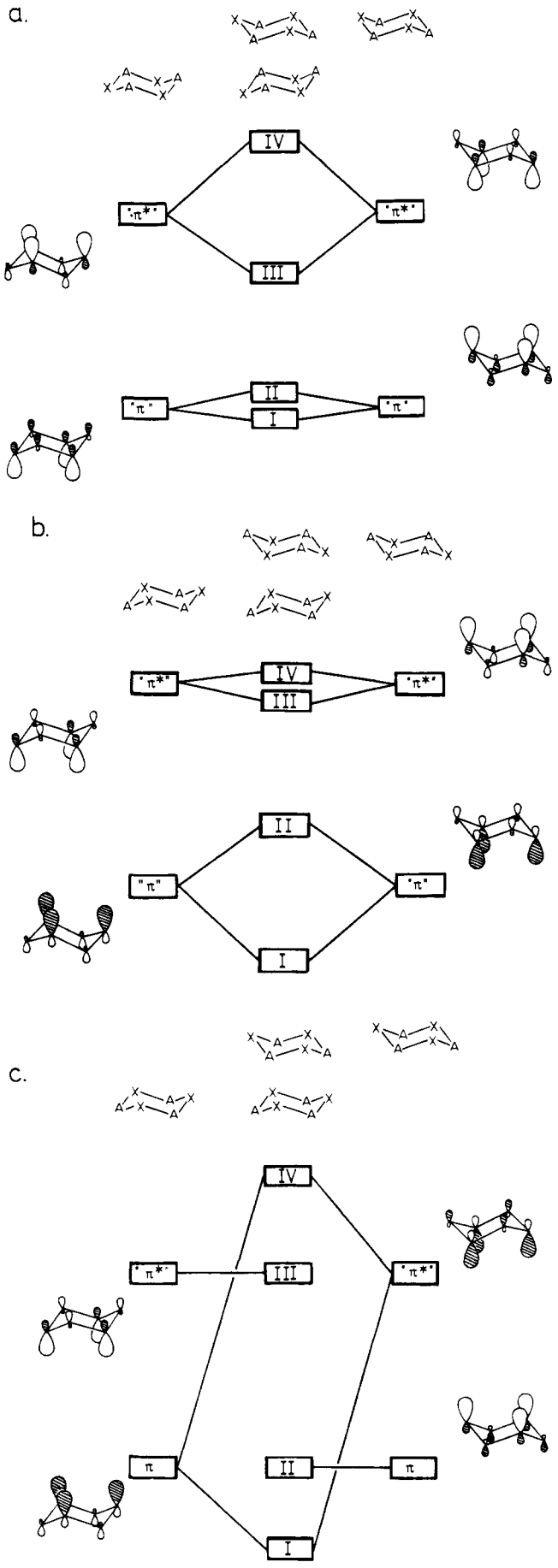

Figure 4. Schematic molecular orbital diagrams for the linking of puckered sheets: (a) AA linkages; (b) XX linkages; (c) AX linkages. (The a_1 orbital in each block is pictorially represented.)

one on top of the next, puckered sheets of atoms appear in the vertical plane (Figure 3). In the sphalerite structure they are in the chair conformation and in the wurtzite structure they are in the boat conformation.

In the AX system there are three ways of arranging these sheets, with AA, XX, and AX intersheet linkages. Figure 4 shows a schematic molecular orbital diagram for interactions of the three types derived by allowing the frontier orbitals of each sheet to interact. We enclose in blocks the three orbitals derived from the π and π^* orbitals of the planar fragment. Thus each rectangular block of orbitals in the diagrams of Figure 4 contains one a_1 and one e species orbital and each will be filled with a total of six electrons. In the AA case, because the lower energy set of outward pointing orbitals on a chair ring is associated largely with the orbitals on the X atoms and points away from the adjacent sheet, the energy changes associated with them are small. These lead to the orbitals labeled I and II. The largest energy changes are associated with the higher energy set of orbitals, largely A located. The result is a set of three AA bonding orbitals (III) and a set of three AA antibonding orbitals (IV). The converse is true for the case where the two sheets are linked by the X atoms. Here the largely X located orbitals interact the strongest leading to XX bonding (I) and antibonding (II) trios of orbitals. The higher energy (largely A located orbitals) point away from the adjacent sheet and remain approximately intersheet nonbonding. (Our diagrams are schematic and aim to emphasize the dominant energy changes on linking the sheets.) For the third case where AX linkages occur then the largest interactions are between high-energy orbitals on one sheet (largely A localized) with low-energy orbitals on the other (largely X localized). The remaining low-energy orbital on one sheet is ready to interact with a high-energy orbital on the next. Using the criterion that electrons in strongly antibonding orbitals lead to structural instability we can readily see that the AA linked structure is favored for nine electrons per formula unit. (With n electrons per AX formula unit the "benzene" molecule of Figure 1 has the configuration π^0, π^3, π^6, $\pi^6\pi^{*3}$, $\pi^6\pi^{*6}$ for n = 6, 7, 8, 9, and 10). This leads to an electron configuration $I^6II^6III^6$. The AX linked arrangement is favored for eight electrons with the configuration I^6II^6 and the XX linked arrangement for seven electrons per formula unit to give the configuration I^6. These ideas are supported by quantitative calculations on pairs of eclipsed chairs. In agreement with these ideas, such structural features are indeed observed, where predicted. In the Cu^IS and Cu^ISe regions of the isomorphous covellite and klockmannite ($Cu^I_2Cu^{II}S_3(Se_3)$) structures chalcogen linked (XX) sheets are found (Figure 5). In both wurtzite and sphalerite modifications (Figure 3) of ZnS and in all other AX systems with this structure and superstructures derived from them, all of which have eight electrons per formula unit, AX linkages are found. Thus AlSb, CuI, and $LiGaO_2$ contain $AlSb_4$, CuI_4, and LiO_4 and GaO_4 tetrahedra, respectively. In the nine-electron GaS and GaSe structures (Figure 6) AA linkages are found. These results are good evidence for covalent directional interaction between the atoms, i.e., electronic control of the geometry. With ten electrons per atom pair the electron configuration is $I^6II^6III^6IV^6$ and none of the three modes of attachment gives rise to bound pairs of sheets. Thus the arsenic structure consists of isolated puckered sheets with intrasheet As–As distances of 2.51 Å and intersheet distances of 3.15 Å. In isomorphous Sb and Bi the corresponding distances are 2.87, 3.37 and 3.10, 3.47 Å. In the next sections we look at the electronic structures of these systems in more detail.

Sphalerite and Wurtzite Structures

Many systems adopt the cubic sphalerite (zincblende) or hexagonal wurtzite structure. It is readily appreciated that with one electron in each of the localized orbitals of **2** then an infi-

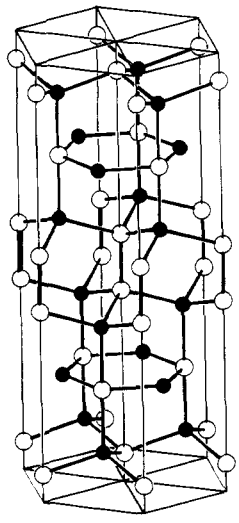

Figure 5. The structure of covellite CuS (solid circles, Cu; open circles, S). There are two nonequivalent copper atoms and the structure is usually regarded as $Cu^{I}_2Cu^{II}S_3$. The "Cu^{I}" atoms are four coordinate and "Cu^{II}" atoms three coordinate.

nite three-dimensional array based on linked puckered sheets is possible with each atom in tetrahedral coordination. This corresponds to an average of four electrons per atom or eight electrons per AX unit according to the Grimm–Sommerfeld valence rule.[12] In addition to elemental carbon these structures are also found for CuCl, HgS, AlN, SiC, etc. If the composition formula of the material is written $0_a1_b2_c \ldots 7_n(N_n)$ where the subscripts (n) represent the number of atoms contributing N electrons, then in general a necessary condition for a tetrahedral structure is that

$$\frac{\sum_{N=0}^{7} nN_n}{\sum n} = 4 \qquad (1)$$

0 refers to a vacancy (or defect) in the structure represented as □. Thus CuCl ≡ 1_17_1, HgS ≡ 2_16_1, AlN ≡ 3_15_1, etc., the defect sphalerite superstructure of $Cd□Al_2S_4$ is equivalent to $0_12_13_26_4$, and the mineral nowackiite,[19] $Cu_6Zn_3As_4S_{12}$ (which has a simple defect sphalerite superstructure), may be written $0_11_62_35_46_{12}$. As we have pointed out[6] there are strong resemblances between the electron-counting procedures here and those determining closo, nido, etc., structures in molecular polyhedra. Many structures are based on these basic arrangements with the addition of spacers between these atoms. Thus the structures of β-cristobalite and β-tridymite (SiO_2) contain Si atoms in the zinc and sulfur positions of sphalerite and wurtzite with 0 atoms between each Si atom; NH_4F has N and F atoms in the zinc and sulfur positions in wurtzite with the H atoms between them. Ice has several crystalline forms of which two contain 0 atoms in the zinc and sulfur positions in sphalerite and wurtzite with H atoms between them.

These two simple tetrahedrally based structures may be viewed in many different ways. As we have noted above we may stress the orientation of adjacent puckered sheets (staggered or eclipsed). Alternatively the sphalerite structure consists only of rings in the chair conformation but the wurtzite structure consists of chairs and boats. (It is not possible to generate a tetrahedral AX structure made solely of rings in the boat conformation.) We could also view the structures via the basic building blocks of **3** and **4**[20] where we show the two symmetry unrelated bond lengths (r_0, r_v) in the wurtzite case. The wurtzite structure is often regarded as a metastable version of the sphalerite arrangement and is found in a relatively small region of the four-coordinate area of Pearson's $\bar{n}$ vs. $\Delta\chi$ diagrams[21] (plots of average principal quantum number vs.

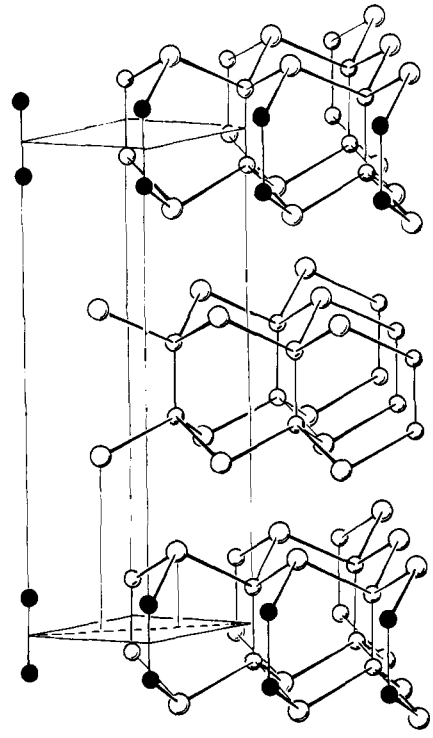

Figure 6. The structure of βGaSe. The α form and the structure of GaS differ from this arrangement by alternative packing of the slabs (large circles, sulfur). The structure is derived from that of wurtzite by fission of apical linkages of wurtzite cages.

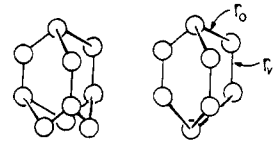

3 4

electronegativity difference). In general it is found for those four-coordinate structures with the largest electronegativity difference between A and X. In the "ideal" wurtzite structure the ratio of the cell parameters $\gamma = c/a = \sqrt{8/3}$ and u, the other variable determining the structure ($r_v = \gamma au = cu$), is equal to $\frac{3}{8}$. The two symmetry unequivalent distances (vertical and oblique) in the cage (**4**) are then given by $r_v = 0.6124a$ (the AX distance parallel to the c axis) and $r_0 = 0.5907a$. The vertical bonds (r_v) are the bonds d of the vertical sheets built from boat conformed rings (**5**). The oblique bonds (r_0) are

5

those (a, b) of the horizontal sheets built from chair fragments (**5**) or alternatively the bonds c of the boat fragments. We have performed calculations on fragments of the sphalerite and wurtzite lattices of varying sizes and on the six-membered rings both terminated by hydrogen atoms. In calculations on largish sphalerite and wurtzite fragments (which necessitate the inclusion of different numbers of atoms to model their local symmetry) the absolute energies are not directly comparable (we shall describe ways to overcome this problem in a future publication) but the energy difference between the two AX structures decreases as the electronegativity of X increases. In calculations on the six-membered rings we always find the chair form more stable but the energy difference decreases as the electronegativity of X increases. (This does not of course mean that the sphalerite form will always be most stable since

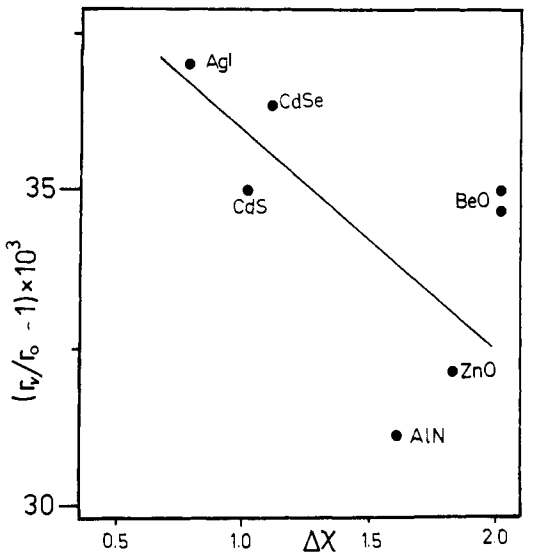

Figure 7. Plot of $(r_v - r_0)/r_0 \times 10^3$ against difference in electronegativity between A and X ($\Delta\chi$) for a collection of AX wurtzite structures for which accurate data is available. (Allred-Rochow electronegativities are used; the plot is similar if Pauling values are substituted.) The two entries for BeO represent determinations at two different temperatures. A plot of the opposite slope is obtained if crystallographic u parameters, uncorrected for anharmonicity, are used instead. See ref 24b. The straight line shows the general trend in these values with $\Delta\chi$.

we are only viewing a very small part of the structure.) In addition bending away from the planar structure becomes less costly. These results are in accord with the prevalence of the wurtzite form in systems with nonzero differences in electronegativity between A and X.[21] The results also fit with previous calculations[22] on cyclohexane and tricycloborazane where the chair form is always found to be more stable than the boat but because of a nonbonded attraction[23] across the ring in the hetero case the energy difference is smaller for $B_3N_3H_{12}$ than in C_6H_{12}. A population analysis for the six-membered ring C_6H_{12} building blocks in the eight-electron case is shown in **6** and predicts $r_v(wz) > r(sp) > r_0(wz)$. Similar values are

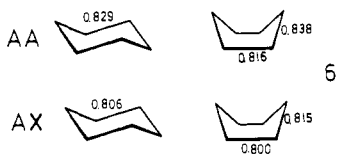

6

found in larger sphalerite and wurtzite fragments. Table I shows bond-length data for the three systems where accurate results are available and the agreement is good. There are many other systems[27] which only show the wurtzite structure and here $r_v > r_0$. The bond-length trends are thus in the directions dictated by electronic considerations. On increasing the electronegativity difference between A and X we find a larger drop in the overlap population for the oblique linkage than the vertical one. As the electronegativity difference increases, therefore, the oblique and vertical linkages become more equal in length. Figure 7 shows a plot of $r_v/r_0 - 1$ for a series of systems against $\Delta\chi$ and the result is in accord with that predicted from the simple calculation on the six-membered ring. Eventually as $\Delta\chi$ increases the Pearson diagrams show that the rock salt (NaCl) structure is produced which contains (**7**) both chair and boat conformed rings. (A change of coordination number to six and change in the geometry of the puckered has also occurred, of course.) Here also the two linkages r_v and r_0 of the wurtzite boats are equal. O'Keeffe and Hyde have used a nonbonded repulsion model[27] based on Bartell and Glidewell's one-angle radii[28] to view this problem. Among the conclusions were that the stability of the wurtzite

Table I. Bond Lengths in Wurtzites and Sphalerites[a] (Å)

	r_0(wz)	r(sp)	r_v(wz)	ref
CdS	2.433(2)	2.527(2)	2.528(2)	24
CdSe	2.540(2)	2.620(2)	2.632(2)	25
AgI	2.713(12)	2.809(2)	2.813(12)	26

[a] Calculated from the crystallographically determined a, c, and u (wurtzite) and a (sphalerite) parameters. Probable errors in parentheses.

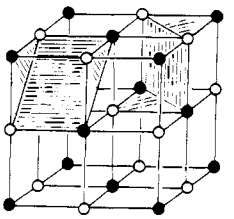

7

compared to the sphalerite form was related to cation-cation (nonbonded AA) interactions in the solid. In this work we have clearly demonstrated that electronic considerations may also account for these structural trends. We do, however, note that significant negative (i.e., repulsive) bond overlap populations have been found between nonbonded atoms in molecular orbital studies. This is seen, for example, between the Mg and Si atoms in SCF NEMO calculations[29] on $H_{10}MgSiO_8$ designed to simulate the environment in forsterite.

A system related to the ones we have discussed is that of polymeric $(CF)_n$. This consists of single puckered sheets with a fluorine atom coordinated to each carbon atom. Both boat and chair conformations of the sheet are possible and, although the evidence is not clear-cut, it is probable that the species is in the chair form, predicted to be of lower energy.

Species with More Than Eight Electrons

We have shown elsewhere[6] how the structures of several electron-rich systems with more than eight electrons per AX unit may be understood via bond-breaking processes of electron-precise wurtzite structure. One of the criteria for structural stability is occupation of all low-energy molecular orbitals and the presence of a large gap between highest occupied and lowest unoccupied molecular orbitals (HOMO and LUMO). Occupation of high-energy orbitals is energetically unfavorable and the system will distort, if able, to lower the energy of the HOMO and increase the HOMO-LUMO gap. Figure 1 showed distortion of the planar to puckered ring, energetically advantageous in the ten-electron case of elemental arsenic, but the basic features of the diagram are found, for example, in the pyramidalization of planar NH_3.[30] A nonbonding or antibonding pair of electrons becomes a bonding pair or lone pair on distortion. In molecules such distortions are often viewed using the second-order Jahn-Teller theorem.[31]

With nine electrons per AX pair (e.g., GaS) if the wurtzite structure were maintained then the extra electrons occupy high-energy orbitals. Following our philosophy, the system should distort, either via an angle or bond distance change, to reduce the energy of these electrons. Figure 8 shows how the molecular orbital energies of a wurtzite cage fragment change during distortion via loss of two "apical" atoms from the structure. A similar diagram is found for another important route—loss of "tropical" atoms from the cage. In both cases an orbital which is cage-terminal atom antibonding becomes a lone pair on the cage, and two deeper lying orbitals become associated with terminator atom orbitals. In each case the highest energy electrons in the nine-electron system are stabilized on distortion. Both of these fragmentation modes are found in practice, in GaS and GaSe (Figure 6) and in the minerals wolfsbergite[32] ($CuSbS_2$) and emplectite[33] ($CuAsS_2$)

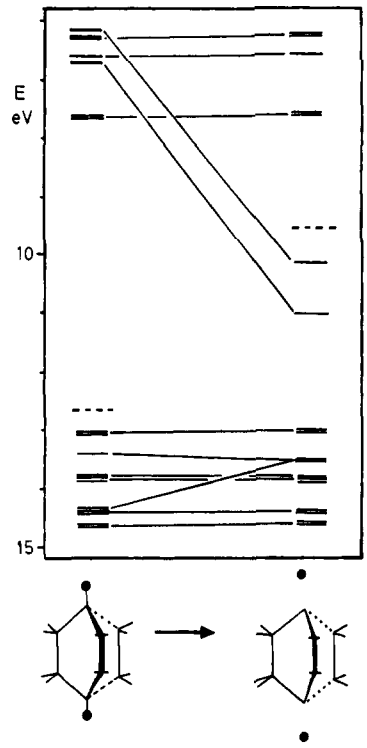

Figure 8. Change in energy of the frontier orbitals of a wurtzite fragment on loss of two apical atoms. (A similar diagram applies for loss of tropical atoms.) A dashed line is drawn above the HOMO corresponding to the eight-electron (ZnS) and nine-electron (GaS) configurations. The two high-energy orbitals which are stabilized become lone pairs on the GaS fragment. The two deeper lying orbitals of the diagram which change energy on distortion become lone-pair orbitals associated with the two detached apical atoms.

(Figure 9). In GaSe, each Ga is tetrahedrally coordinated by one Ga and three S atoms and each S atom is pyramidally three coordinated by Ga. The GaS and GaSe structures only differ in the way the fragmented slabs are oriented with respect to each other. One very striking feature is that a rearrangement of atom positions within each wurtzite cage has occurred such that Ga–Ga pairs are found and the electronegative sulfur atom is three coordinate. We return to this point shortly.

If the wolfsbergite and emplectite structures are written as $Cu^{I}B^{III}S_2$ (B = Sb, As) to satisfy valence rules, then the number of electrons on average per AX unit is $(1 + 5)/(2) + 6 = 9$ and the system is isoelectronic with GaS. Here the Cu atoms are four coordinate, and the Sb atoms and half the sulfur atoms three coordinate. Rupture of apical *and* tropical linkages in each cage will not lead in general to easily viewed slab structures as we have described.

The population analysis from a calculation on a fragment of a GaS slab (where all the atoms are made the same and the total number of electrons adjusted to reproduce the nine-electron AX case) is shown in **8** and clearly shows that the

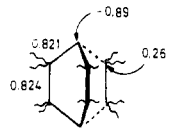

8

apical atoms of each cage carry the highest charge. Using ideas now well established in viewing the structures of molecules, the most electronegative species will occupy these sites, in this case the sulfur atoms.[34] Calculations on systems where the various alternatives of atomic arrangements are included leads to the same conclusion on an energetic basis. Thus both these ways of viewing the structure, either from the charge control aspect outlined here or via the energetics of the interacting

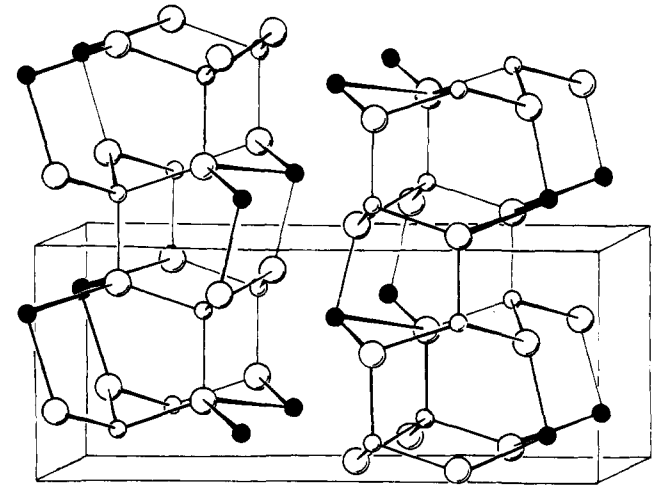

Figure 9. The structure of wolfsbergite ($CuSbS_2$) (large circles, sulfur; small open circles, copper). Emplectite ($CuAsS_2$) is isostructural. The structure is derived from that of wurtzite by fission of tropical linkages of wurtzite cages and consists of two-dimensional slabs of the structure shown here continued indefinitely in the vertical direction and the direction perpendicular to the paper.

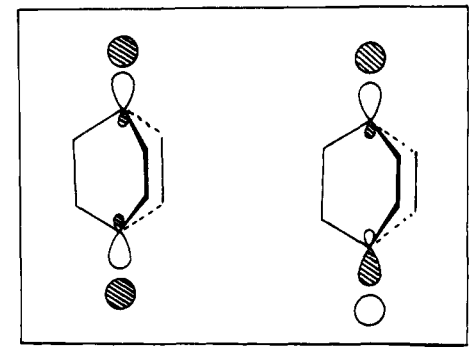

Figure 10. The form of the molecular orbitals of the wurtzite fragment which become lone-pair orbitals (Figure 8) on loss of two apical atoms (There are small contributions from other atomic orbitals which are not shown.)

sheets, predict that the sulfur atoms should occupy the apical sites. Previous considerations of this problem have emphasized the importance of metal–metal bonding which of course also may be a factor. We do note, however, that the population analysis shows little difference in bond overlap population between the symmetry-unrelated linkages. In the wolfsbergite structure the copper atom remains four coordinate but the more electronegative Sb and half the S atoms are three coordinate.

We may tackle this atom site preference problem in yet another way by taking the molecular orbital diagram of the wurtzite fragment and asking how the electronic nature of the skeletal atoms need to be changed in order that the two lowest unoccupied orbitals in ZnS (and thus the two highest occupied orbitals in GaS) are the ones which are stabilized on distortion by the loss of the two apical ligands. The form of the two orbitals in ZnS which correlate with lone pairs in GaS is shown in Figure 10 and one obvious way of lowering their energy to ensure that they are the orbitals filled in a hypothetical GaS species with the wurtzite structure is to increase the ionization energy of the orbitals on the apical atoms.[35] Thus introduction of electronegative ligands at these apical sites encourages fission of the apical linkages when the number of electrons is increased. Similar considerations would apply to the wolfsbergite structure, but why the wurtzite structure splits apart in one way in one species and in a different way in the other is a question

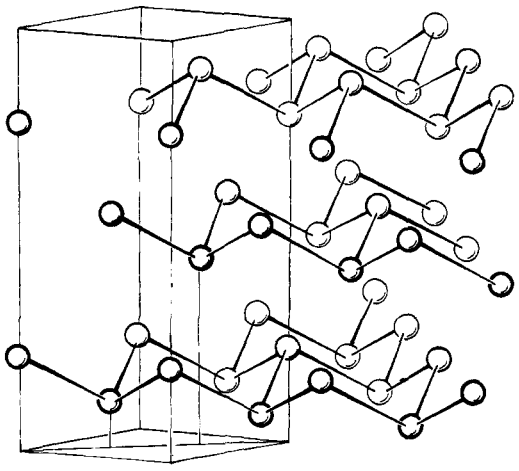

Figure 11. The arsenic structure showing puckered hexagonal sheets of atoms.

which needs more quantitative study than we are prepared to commit with our simple extended Hückel calculations at present.

Interestingly both GaS and $CuSbS_2$ lie in the tetrahedral part of the Pearson diagrams and so, if this empirical scheme applies to these species, then distorted structures based on wurtzite or sphalerite are perhaps to be expected. In fact GaS and GaSe lie inside and $CuSbS_2$ and $CuAsS_2$ just outside the region where wurtzite structures are found in electron-precise structures. (Similarly the structures of several electron-rich sulfides and sulfo salts which would lie in the rock-salt part of the Pearson diagram may be described as distorted rock-salt structures.[36]) Thus the structures of these two electron-rich systems are readily understood using simple molecular orbital ideas.

Arsenic Structure

Whereas GaS contains nine electrons per atom pair, elemental arsenic has ten. Following the bond-breaking approach of the previous section there are two ways the GaS structure may split, vertically or horizontally, or alternatively two ways the wolfsbergite structure may fragment. Splitting the wolfsbergite structure vertically gives a puckered sheet structure composed of boat conformed rings which is not found in any species. Splitting the GaS structure horizontally leads to the layered arsenic structure (Figure 11). Splitting the wolfsbergite structure horizontally or the GaS structure vertically leads to a structure made up of "tubes" of wurtzite cages (**4**) stacked side by side. A related atomic arrangement is found in the tubes comprising the red (or violet) phosphorus structure. Similar fragmentation of the sphalerite structure leads to puckered sheets based on the chair conformation. The overall appearance of the molecular orbital correlation diagram on splitting apart the structure is similar to that of Figure 8. Occupied orbitals (in the ten-electron case) which are antibonding between the peripheral atoms of each sheet drop in energy and become lone pair orbitals on the As layers. In the actual arsenic structure

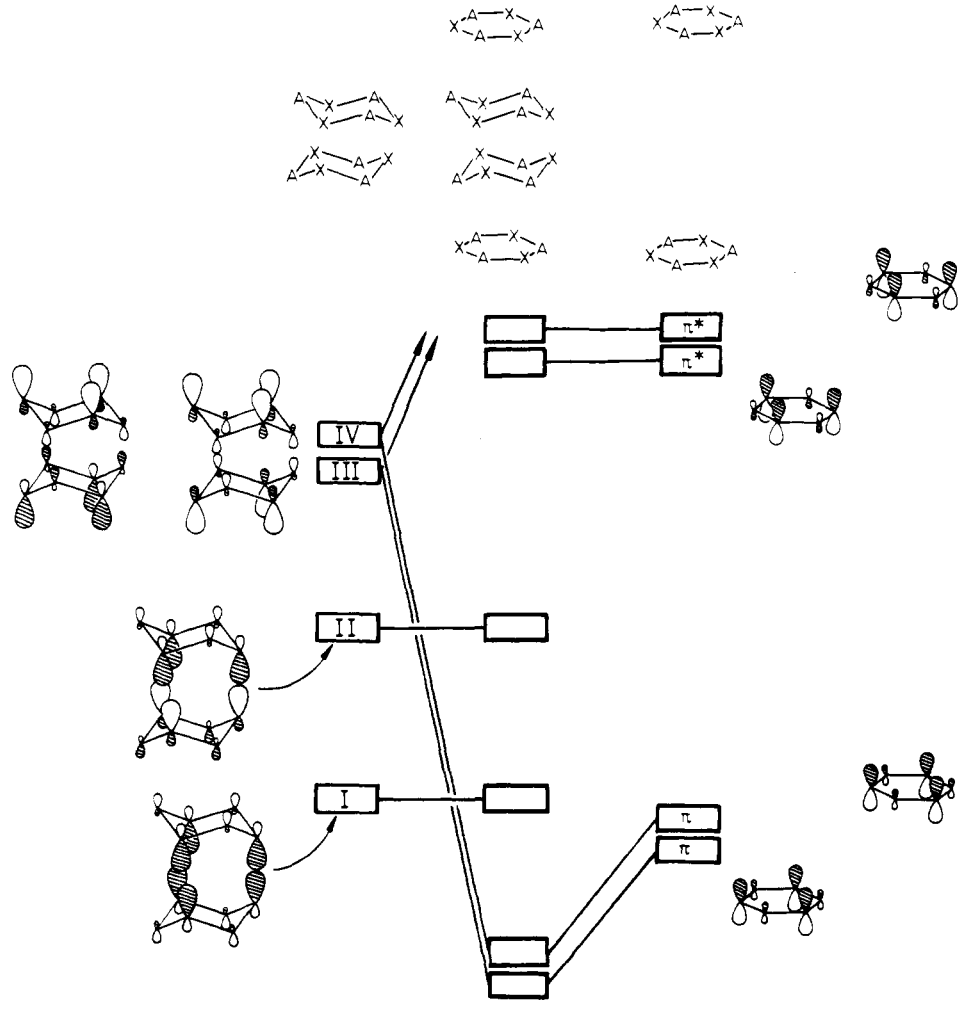

Figure 12. Schematic molecular orbital diagram for the assembly of a fragment of the covellite structure from a GaS fragment and two fragments of a planar sheet. (The a_1 orbitals in each block are pictorially represented.)

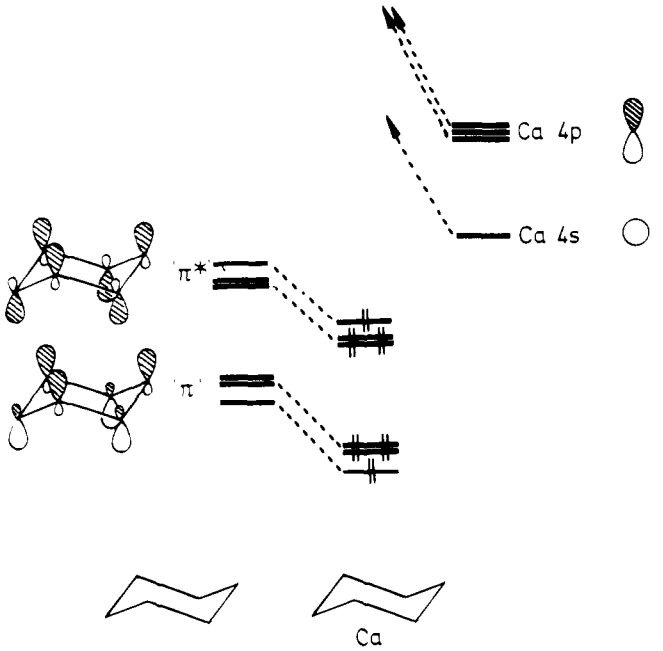

Figure 13. Linking of two puckered sheets by atomic species of low ionization potential as in $CaSi_2$. (An analogous diagram applies to the $CaGa_2$ structure which contains planar sheets.) The diagram shows stabilization of the filled orbitals on the puckered sheet by empty higher energy orbitals of the "Ion". In an exactly analogous fashion the filled orbitals of another sheet are stabilized by completing the sandwich.

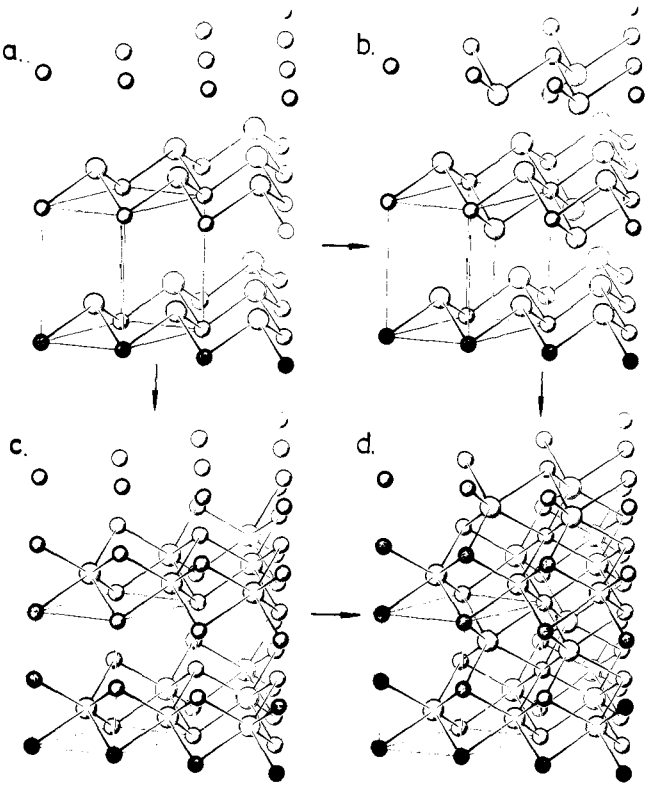

Figure 14. Generation from the puckered sheet (a), of the CdX_2 (b), MoS_2 (c), and NiAs (d) structures via the process of **9**. (As a result of our illustrative assembly procedure the cadmium halide structure contains octahedrally coordinated X rather than A atoms. In the real 16-electron systems with this structure the AX_2 arrangement with octahedrally coordinated A is of course found.) Like many of our diagrams the two-dimensional representation of these three-dimensional structures makes them appear more complex than they really are. We would encourage the reader to use models whenever possible in viewing such solid-state structures.

the sheets have slipped relative to each other to aid in packing. Parthé has viewed[8] this structure as a defect one based on tetrahedral coordination (a 05_4 structure) and in general the bond-breaking and defect approaches are probably just as applicable to view atomic arrangement whether in molecules or solids.

Covellite (CuS) Structure

Now that GaS, arsenic, and graphite structures are understandable we may rationalize the unusual structure of covellite (CuS) and klockmannite (CuSe) shown in Figure 5. The structure may be regarded either as a wurtzite-type structure with a graphite-like spacer between every other puckered layer or GaS slabs and graphite layers stacked alternatively. There are two types of copper atom. Cu(1) is coordinated by three S(1) atoms in a plane and Cu(2) is coordinated by three S(2) and S(1) atoms in near-perfect tetrahedral coordination. S(1) is coordinated by three Cu(1) and two Cu(2) in a trigonal-bipyramidal environment. The axial Cu–S distance (2.34 Å) is longer than the equatorial (2.19 Å) as found in the majority of trigonal bipyramidal AY_5 systems where A is a main-group atom.[37] S(2) is coordinated by three Cu(2) and one S(1) in a nearly tetrahedral environment. The structure is usually regarded as being $Cu^{I}_2Cu^{II}S_3$ with the Cu^{I} atoms occuping the Cu(2) sites.[38] (Tetrahedral Cu^{II} is Jahn–Teller unstable and is unlikely to be found in this environment.) $Cu^{I}S$ has seven electrons and we described above (Figure 4) how puckered sheets with this electron configuration were expected to link via bonds formed between the electronegative atoms (in this case the S atoms). The outward pointing orbitals (I and IV of Figure 12) of such a GaS-type slab, largely copper located, are unoccupied with this particular electron configuration and therefore seek out occupied lower energy orbitals with which to interact. The graphite-like $Cu^{II}S$ sheet is an ideal candidate. With eight electrons per formula unit there are six electrons in the lower energy set of π orbitals. Furthermore, the electron density is largely located on the electronegative sulfur atoms and so the links between the two structures should be (as observed in covellite and klockmannite, Figure 5) via the Cu atoms of the GaS-type slab and the S atoms of the graphite-like sheet. Here overlap is greatest. In Figure 12 we show how one XX linked pair of puckered sheets may interact with a pair of planar sheets to form part of the covellite structure (Figure 4). The occupied low-energy orbitals of this structure are ready to interact with the high-energy orbitals (III and IV) of another pair of XX linked puckered sheets and so the structure is built up. The type of linkages within a sandwich containing one planar sheet enclosed by two puckered sheets is a 3c–2e bond similar to the bridge bonds in Al_2Cl_6. Given the general features of this structure we may then readily understand in simple molecular orbital terms how it is assembled and which atomic species occupy which sites. Why CuS has this structure but ZnS simpler tetrahedral arrangements is a more difficult problem and one we will not tackle here.

Linking Puckered Sheets with Spacers

I. $CaSi_2$ and AlB_2 Structure. The ten-electron $CaSi_2$ structure consists of puckered graphite-like sheets (Si–Si = 2.48 Å) with calcium atoms lying between the sheets with CaSi distances of about 3 Å. An ionic model would regard the structure as being composed of Si^--containing sheets, isoelectronic and isostructural with elemental arsenic held together by Ca^{2+} ions. In molecular orbital terms we can imagine the frontier orbitals of the puckered ring being stabilized by unoccupied high-energy orbitals on the Ca atom (Figure 13). An exactly analogous covalent argument holds to rationalize the AlB_2 structure found for the eight-electron $CaGa_2$, MgB_2 species which could be viewed as arising on an ionic model as Ca^{2+} or Mg^{2+}

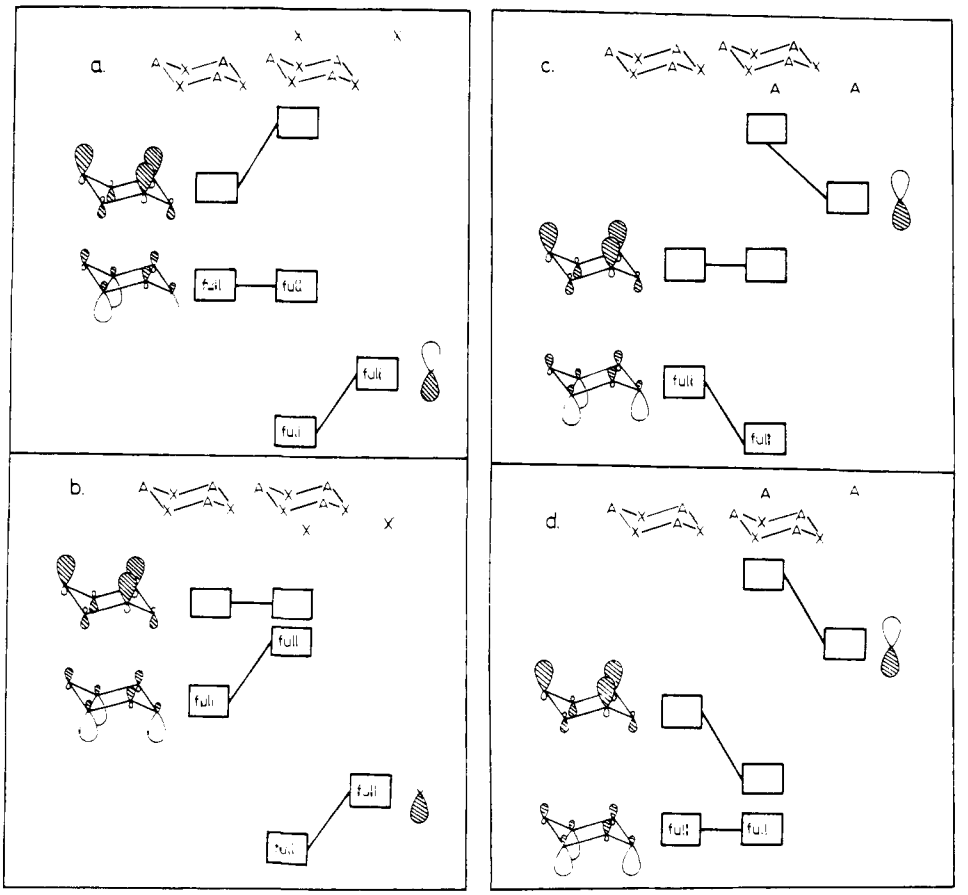

Figure 15. Schematic molecular orbital diagrams showing capping of the puckered sheet to give the cadmium halide structures. The a_1 orbital from each block is pictorially represented. An electronegative atom X capping a puckered AX sheet (a) on the A atom side, (b) on the X atom side. An atom of low electronegativity (A) capping an AX sheet (c) on the X atom side and (d) on the A atom side. The electron occupancy represents in (a) and (b) a Cl^- ion capping a $CdCl^+$ sheet (for example) and in (c) and (d) a Cs^+ ion capping a CsO^- sheet. (b) and (d) are unfavorable arrangements since either occupied orbitals are destabilized (b) or the best stabilization occurs with unoccupied orbitals (d).

ions sandwiched between Ga^- or B^- sheets, isoelectronic with graphite. The effect of the extra pair of electrons is easy to see on moving from $CaGa_2$ to $CaSi_2$. The sheet becomes puckered just as on moving from graphite to arsenic. Neither of these structures is available for $CaCl_2$ or $CdCl_2$ since with 16 electrons these electrons will go into antibonding orbitals which will either split apart the sheets from the sandwiched atoms or break up the puckered sheet itself. The latter feature is found in the structure of the red, tetragonal form of ZnP_2 (12 electrons) where some of the phosphorus atoms form bonds with three neighbors and the others with two.

II. CdX_2, MoS_2, and NiAs Structures. These structures are readily derived via Scheme I, which is shown pictorially in Figure 14. Let us start with the CdX_2 structure. The two structures X = I, Cl basically only differ in the way capped puckered sheets are stacked with respect to each other. Many polymorphs exist differing only in the way the sheets are stacked. These structures are related to the MoS_2 structure simply by the mode of capping the puckered sheet. In the cadmium halide structures each Cd atom is octahedrally six coordinate; in the MoS_2 structure each Mo is trigonally prismatically six coordinate. In both structures the X, S atoms are pyramidally three coordinate. Note that after the capping process the capping X atoms are identical in character with the X atoms initially in the puckered sheet; their differentiation here is purely to help us view the electronic structure of these systems. The geometry of the puckered sheet which receives the capping atoms is slightly different from the one we have used above in that the angles around each atom are 90° rather than tetrahedral. The form of the orbitals is, however, very

Scheme I

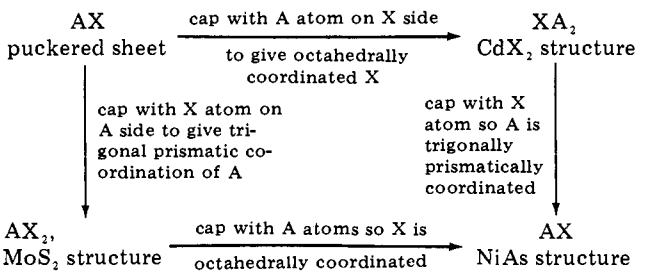

similar to those of Figure 2. In CdX_2 and MoS_2 the extra layer of electronegative X atoms caps the side of the puckered sheet containing the metal atoms. If we regard the structure (for bookkeeping purposes) as being made up of a puckered CdX^+ layer (eight electrons, isoelectronic with graphite) and capping X^- atoms (filled valence orbitals), then we can see why this particular arrangement is most stable (Figure 15). Capping the more electronegative side with the electronegative atoms clearly leads to an energetically unfavorable situation borne out by a calculation on a model system. Again the most electronegative atoms have the lowest coordination number in the resulting structure. Figure 16 shows the result of a molecular orbital calculation on a system designed to model the capping process. For the electronic configuration of CdX_2 there are exactly the right number of electrons to fill the low-energy orbitals. For all the known 16-electron systems with this structure the most electronegative atoms sandwich the more

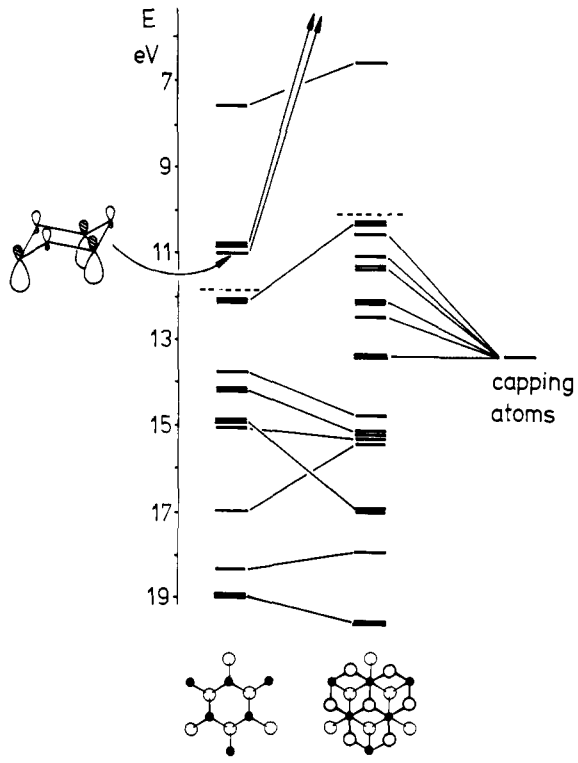

Figure 16. Orbital energy changes on capping a puckered sheet (angles = 90°) to give the cadmium halide structure. The diagram represents the process $A_3X_3H_6$ (eight electrons per AX unit) + XH_6 (all X and H orbitals full) where the X atom symmetrically caps the A_3X_3 unit and the six H atoms occupy symmetry-equivalent (in the extended solid) positions. Note that the π^* derived orbitals of the puckered sheet (mainly A located) are heavily destabilized on capping. (The a_1 orbital of this trio is pictorially represented.) Dashed lines are drawn above the HOMO in each structure. A large HOMO-LUMO gap is naturally produced on capping. The small HOMO-LUMO gap in the puckered sheet gives rise to structural instability and leads to formation of capped (e.g., CdX_2) or linked (e.g., wurtzite or delafossite) structures.

electropositive species. However, the inverse structure is known for eight-electron species, e.g., Cs_2O, and other species with small numbers of electrons. Here the situation is the opposite to the above: the more electropositive species sandwich the electronegative one. We can clearly see, however, that this is just what is expected with this number of electrons (Figure 15) since the maximum stabilization of the electrons in orbitals largely located on the electronegative atom occurs.

It is interesting to view the $CdCl_2$ structure from the point of view of the solid-state analogue of Wade's rules for molecular polyhedra. Locally the structure consists of a cube with one vertex missing (**10**). In cubane (C_8H_8), an electron-precise

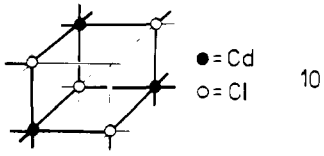

10

molecule, there are 24 skeletal electrons to hold together the 12-sided cube. In the $CdCl_2$ unit there are three six-coordinate Cd atoms with three of the coordinating chlorine atoms in the cage, three three-coordinate chlorine atoms with two of the coordinating cadmium atoms in the cage, and one three-coordinate chlorine atom with all three coordinating cadmium atoms in the cage. Thus the total number of skeletal electrons per pseudocube is $3 \times 2 \times 3/6 + 3 \times 7 \times 2/3 + 1 \times 7 \times 3/3 = 24$, a figure identical with that for cubane. So $CdCl_2$ is a nido structure. $CrCl_3$ has a related geometry with every third metal atom of the $CdCl_2$ structure missing. The chlorine atoms are

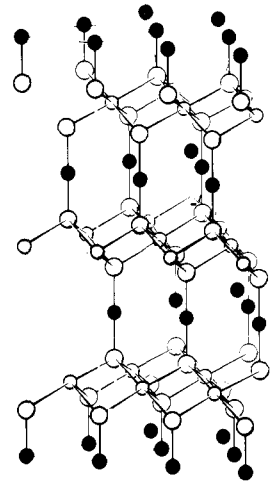

Figure 17. The delafossite structure found for many $M^IM^{III}O_2$ systems (M^I = Cu, Ag, H; M^{III} = Fe, Cr, Ir, etc.). Small solid circles are M^I, small open circles are M^{III} atoms in octahedral coordination, and large circles are O atoms in tetrahedral coordination.

thus two coordinate. Skeletal counting in the pseudocube here gives an electron count of $2 \times 3 \times 3/6 + 2 \times 7 \times 1/2 + 2 \times 7 \times 2/2 = 24$, i.e., an arachno structure. BiI_3 is related to $CrCl_3$ just as CdI_2 is related to $CdCl_2$ (i.e., different packing of the slabs) and may be viewed analogously. Here, however, each Bi atom contributes five electrons to the structure whereas Cr only contributed three. The structure only fits into the scheme if the Bi atom contains a stereochemically inert pair of electrons. This is often found in octahedrally coordinated Bi complexes and species with a heavy central atom from the right-hand side of the periodic table. $Bi^{III}X_6^{3-}$ species, with seven pairs of electrons, are octahedral species as are several Te^{IV} species.

If the NiAs structure (Figure 14) is written as $Ni^{III}As$, then for bookkeeping purposes the CdX_2-like sheets may be regarded as 16-electron $NiAs_2^{3-}$ systems, and the linking process b → d of Figure 14 is equivalent to the linking of single puckered sheets by metal atoms in the $CaSi_2$ structure. In the actual structure, of course, there is no difference between the metal atoms to which we assign different roles in the aufbau process.

III. Delafossite ($CuFeO_2$) Structure. There are numerous oxides with this structure (Figure 17) of general formula M^I-$M^{III}O_2$. It is simply related to the cadmium halide structure in that the X atoms of adjacent CdX_2 slabs containing $M^{III}O_2$ are bridged by M^I atoms. Thus each M^{III} atom is in octahedral coordination, by six O atoms, each O atom is tetrahedrally coordinated by three M^{III} and one M^I atoms, and each M^I atom (Cu or Ag) is linearly two coordinated by O. $HNaF_2$ has an analogous structure with the NaF_2 unit comprising the CdX_2 slab and bridging H atoms. The orbital picture is similar to that for the other linked systems we have discussed. For bookkeeping purposes $M^{III}O_2^-$ or NaF_2^- slabs (isoelectronic with $CdCl_2$) are held together by M^+ or H^+ species. In molecular orbital terms the (empty) higher energy orbitals on M^+ or H^+ may interact with and stabilize the (full) lower energy orbitals on the O atoms. This structure will be particularly favored for those cases where the M^I or H species has a tendency for two coordination.

Discussion

The structures of many solid materials are often considered as being held together by ionic forces with some covalent character added in. The predictive value of thermochemical electrostatic lattice energy calculations using an ionic model in rationalizing solubilities, thermal decomposition tempera

ture, etc., is now well established following the work of Kapustinskii.[40] However, use of radius ratio rules to view the structures of even the alkali halides is very unsatisfactory.[41] Fifty percent of the room temperature/pressure structures are predicted incorrectly. A review by Dunitz and Orgel[42] in 1960 entitled "The Stereochemistry of Ionic Solids" used crystal-field theory (ionic interactions between metal and ligand) to rationalize the structures of many solids containing transition metals. However, we have recently shown that all of these classic crystal-field results may be achieved by using (covalent) molecular orbital theory and in just a simple fashion.[43,44] (This does not mean, of course, that ionic forces are nonexistent.) We show elsewhere[36] that the TlI and PbO structures, among others viewed by these authors in ionic terms, have ready rationalization in covalent, molecular orbital terms. The major problem in the past in using covalent ideas to view solid-state structures has been the choice of the unit on which the molecular orbital calculation has been performed. Most progress has been made in viewing tetrahedral structures where four localized orbitals (sp^3 hybrids using the language of Pauling) may be readily envisaged. But we have shown here that the fragment approach may just as readily be used to view the "capped" puckered sheet (the cadmium halide structures) containing octahedrally coordinated metal atoms without any additional modifications.

What then are the important factors in determining the structures of these materials? Hyde and O'Keeffe have rationalized[27] the prevalence of the wurtzite AX structure at nonzero values of $\Delta\chi$ using a nonbonded model as we noted above. Using an ionic model we could understand the same result. In hetero systems there are larger trans ring attractions[45] in rings with the boat compared to the chair conformation. This stabilization increases with increasing ionicity (i.e., $\Delta\chi$).[46] In this paper we have shown that purely covalent effects give rise to similar stabilization of boat-form rings as $\Delta\chi$ increases. All three factors may be important. As a general approach to view the structures of solids clearly the covalent approach is a good one. At the qualitative level it is able to follow the breakup of structure as the number of electrons is increased. It also shows for closed-shell systems why the most electronegative atoms occupy the sites of lowest coordination number and why S–S linkages are found in covellite but Ga–Ga linkages in GaS. An ionic or nonbonded repulsion model has difficulty in convincingly rationalizing these structural observations. At the quantitative level the covalent electronic approach is able to rationalize changes in interatomic distances and the relative stability of AX wurtzites and sphalerite structures with the nature of A and X.

Acknowledgment. This work has benefited by conversations with Professors P. B. Moore and J. V. Smith.

Appendix

The extended Hückel calculations[22] were performed on systems containing (A=) carbon atoms (H_{ii} values in eV and exponents in parentheses) 2s 21.4 (1.625), 2p 11.4 (1.625). A more electronegative atom (X) was simulated by increasing both H_{ii} values by 3 eV. The hydrogen parameters were 13.6 eV (1.300) and all bonded AA, AX, XX, and XH distances were fixed at 1.5 Å for all calculations.

References and Notes

(1) Fellow of the Alfred P. Sloan Foundation.
(2) See, for example, N. B. Hannay, Ed., "Treatise on Solid State Chemistry", Vol. 1-6, Plenum Press, New York, 1974.
(3) (a) J. C. Phillips. "Covalent Bonding in Crystals, Molecules and Polymers", University of Chicago Press, Chicago 1969; (b) J. B. Goodenough "Magnetism and the Chemical Bond", Wiley, New York, 1963.
(4) For example, (a) J. A. Tossell, D. J. Vaughan, and K. H. Johnson, *Chem. Phys. Lett.*, **20**, 329 (1973); (b) J. A. Tossell, *J. Electron Spectrosc. Relat. Phenom.*, **8**, 1 (1976); *Am. Mineral.*, **61**, 130 (1976).
(5) For example, (a) S. J. Louisnathan and G. V. Gibbs, *Am. Mineral.*, **57**, 1643 (1972); G. A. Lager and G. V. Gibbs, *Ibid.*, **58**, 756 (1973); (b) J. K. Burdett, *Inorg. Chem.*, **18**, 1024 (1979).
(6) J. K. Burdett, *Nature (London)*, **279**, 121 (1979).
(7) K. Wade, *Adv. Inorg. Chem. Radiochem.*, **18**, 1 (1976).
(8) E. Parthé, "Crystal Chemistry of Tetrahedral Structures", Gordon and Breach, New York, 1964.
(9) D. M. P. Mingos, *Nature (London)*, *Phys. Sci.*, **236**, 99 (1972).
(10) M. Elian and R. Hoffmann, *Inorg. Chem.*, **14**, 1058 (1975).
(11) For a discussion of the Schäfli notation see ref 12.
(12) R. B. Pearson, "The Crystal Chemistry and Physics of Metals and Alloys", Wiley, New York, 1972.
(13) L. Pauling, "The Nature of the Chemical Bond", 3rd ed., Cornell University Press, Ithaca, N.Y., 1960.
(14) See, for example, D. Schonland, "Molecular Symmetry", Van Nostrand, Princeton, N.J., 1965.
(15) The structures of many of the systems we will discuss appear in several standard reference works and will not be separately referenced. We refer the reader to refs 12 and 16.
(16) A. F. Wells, "Structural Inorganic Chemistry", 4th ed., Oxford University Press, London, 1975.
(17) L. G. Berry, *Am. Mineral.*, **39**, 504 (1954).
(18) Z. S. Basinski, D. B. Dove, and E. Mooser, *Helv. Phys. Acta*, **34**, 373 (1961).
(19) F. Marumo, *Z. Kristallogr., Kristallgeom., Kristallphys., Kristallchem.*, **124**, 352 (1967).
(20) Another way is to view the structure via the packing of tetrahedra. See T. Zoltai, "Systematics of Sulfide Mineralogy", University of Minnesota, unpublished, 1974.
(21) W. B. Pearson, *J. Phys. Chem. Solids*, **23**, 103 (1962).
(22) R. Hoffmann, *J. Chem. Phys.*, **39**, 1397 (1963); **40**, 2474 (1964).
(23) R. O. Buttlar, D. F. Gaines, and R. Schaeffer, *Adv. Chem. Ser.*, **No. 42** (1963).
(24) (a) J. Castles, private communication in (b) S. L. Mair and Z. Barnea, *Acta Crystallogr., Sect. A*, **31**, 201 (1975).
(25) Z. Barnea, Ph.D. Thesis, University of Melbourne, 1973.
(26) J. Burley, *J. Chem. Phys.*, **38**, 2807 (1963).
(27) M. O'Keeffe and B. G. Hyde, *Acta Crystallogr., Sect. B*, **34**, 3519 (1978).
(28) C. Glidewell, *Inorg. Chim. Acta*, **12**, 219 (1975).
(29) J. A. Tossell and G. V. Gibbs, *Phys. Chem. Miner.* **2**, 21 (1977).
(30) See, for example, B. M. Gimarc, "Molecular Structure and Bonding", Academic Press, New York, 1979.
(31) (a) L. S. Bartell, *J. Chem. Educ.*, **45**, 754 (1968); (b) R. G. Pearson, *J. Am. Chem. Soc.*, **91**, 1252, 4947 (1969).
(32) W. Hofmann, *Z, Kristallogr., Kristallgeom., Kristallphys., Kristallchem.*, **84**, 177 (1933).
(33) J. C. Portheine and W. Nowacki, *Z. Kristallogr., Kristallogeom., Kristallphys., Kristallchem.*, **141**, 387 (1975).
(34) In general sites of lowest coordination carry the highest charge (as seen in **8**). Taken to the extreme limit ClF_3 has a central Cl rather than central F atom because the sites which are one-coordinate carry the highest charge and attract the most electronegative ligands.
(35) The factors influencing the energies of antibonding orbitals are discussed in J. K. Burdett, *J. Am. Chem. Soc.*, **101**, 580 (1979).
(36) J. K. Burdett, in preparation.
(37) R. Hoffmann, J. M. Howell, and E. L. Muetterties, *J. Am. Chem. Soc.*, **94**, 3047 (1972).
(38) We note here the general problem of assigning oxidation states in solids. These species have long been regarded as containing Cu^{I} and Cu^{II} (Figure 5) and this is how we shall regard them. Recent XPS studies, however, have found only a single Cu 2s peak in the region associated with Cu^{I} (H. Rupp and U. Weser, *Bioinorg. Chem.*, **6**, 45 (1976)) and the detailed electronic structure is clearly quite complex (J.A. Tossell, *Phys. Chem. Miner.* **2**, 225 (1978)). Our artificial way of looking at the structure uses the Cu^{I}/Cu^{II} viewpoint simply for bookkeeping purposes.
(39) B. J. Wuensch in "Sulfide Mineralogy", Mineralogical Society of America, Washington, D.C., 1974.
(40) (a) A. F. Kapustinskii, *Q. Rev., Chem. Soc.*, **10**, 283 (1956); (b) T. C. Waddington, *Adv. Inorg. Chem. Radiochem.*, **1**, 157 (1959); (c) D. A. Johnson, "Thermodynamic Aspects of Inorganic Chemistry", Cambridge University Press, New York, 1968.
(41) See the discussions (a) J. C. Phillips in ref 2, Vol. 1, p. 1; (b) J. E. Huheey, "Inorganic Chemistry", 2nd ed., Harper and Row, New York, 1978.
(42) J. D. Dunitz and L. E. Orgel, *Adv. Inorg. Chem. Radiochem.*, **2**, 1 (1960).
(43) J. K. Burdett, *Adv. Inorg. Chem. Radiochem.*, **21**, 113 (1978).
(44) J. K. Burdett, *Chem. Soc. Rev.*, 7, 507 (1978).
(45) The charge distribution in solid ZnO has been calculated by J. R. Chelikowsky, *Solid State Commun.*, **22**, 351 (1977).
(46) A similar structure dependence on an "experimental" ionicity obtained via photoelectron spectroscopy has been found by S. P. Kowalczyk, L. Ley, F. R. McFeely, and D. A. Shirley, *J. Chem. Phys.*, **61**, 2850 (1974).